Preparation and Corrosion Resistance of Micro-arc Oxidation/Self-Assembly Composite Film on 6061 Aluminum Alloy

Ming Ming Ma, Yu Qing Wen, Wei Shang*, Jia Ping Li*

Guilin University of Technology, No. 12, Jiangan Road, Guilin City, Guangxi, China.
*E-mail: 2006027@glut.edu.cn

The aluminum alloy has some advantages and has wide application in modern life. However, aluminum alloys are easily corroded by corrosive substances in the environment, thus affecting their service life. In order to improve the corrosion resistance of the aluminum alloy surface, The composite film was prepared by micro-arc oxidation, self-assembly and doping, which were micro-arc oxidation (MAO), bis[3-(triethoxysilyl)propyl]tetrasulfide(BTESPT) and graphene oxide (GO). The morphology and composition of the composite film (MAO/BTESPT/GO) were tested by SEM, EDS. The salt spray test, Tafel polarization curve and electrochemical AC impedance were used to test the corrosion resistance of the composite film. The results shown that the micro-arc oxidation-self-assembled composite film had excellent corrosion resistance. And the corrosion current density of the composite film was reduced by 5 orders of magnitude compared with the substrate. The salt spray test results shown that the corrosion resistance of the composite film was greatly improved compared with that of the matrix and the self-assembled film. The composite film exhibited excellent corrosion resistance.

1. INTRODUCTION

Aluminum and its alloys have the advantages of low density, good mechanical properties, light weight, high strength and good plasticity[1]. It has been widely and successfully applied in engineering fields such as aviation industry[2-5], construction industry[6] and automobile industry[7]. However, in an environment with a humidity of 50% or more, it is easy to contact with moisture and dust particles in the environment. Most of the dust particles contain some small amounts of metal ions, and some elements in the aluminum alloy are also susceptible to moisture in the air, thereby forming a primary battery, resulting in electrochemical corrosion behavior of the aluminum alloy matrix. Therefore, it

causes a large economic loss to the world every year. In order to reduce the economic loss of the world, it is necessary to improve the corrosion resistance of the aluminum alloy. Metal surface protection and corrosion protection methods are currently available in a variety of ways, and the reaction types can be roughly divided into three types: chemical[8-10], electrochemistry[11] and physical treatment. There are many methods of chemical treatment, and there are three main types: organic film treatment[12-14], phosphate conversion film [15] and chromate passivation film[16-19]; electrochemical treatment includes: anodizing[20-22] and micro-arc oxidation[23-25]; physical treatment includes: organic solvent cleaning and mechanical grinding. Micro-arc oxidation is developed on the basis of traditional anodization. The micro-arc oxidation process consists of two reactions, an electrochemical reaction and a plasma chemical reaction. Zhan [26] studied the electroless nickel plating on the basis of microarc oxidation of magnesium alloy. The research shown that nickel plating on the micro-arc oxidation film can well protect the magnesium alloy matrix. M. Mohedano [27] added the σ-Al_2O_3 phase in the electrolyte to increase the content of the σ-Al_2O_3 phase of the micro-arc oxidation film of the aluminum alloy, thereby improving the hardness and wear resistance of the micro-arc oxidation film of the aluminum alloy. In recent years, micro-arc oxidation technology has many mature processes, which have attracted extensive attention in the surface treatment of aluminum alloys. Although the micro-arc oxide film can prevent the corrosion of the aluminum alloy to some extent. However, there are many micropores and microcracks on the surface of the micro-arc oxide film, which hinders its application to the corrosion protection of aluminum alloys.

Graphene has broad application prospects in experimental research and industrial applications. It has a unique structure and excellent physical and chemical properties. It is a new type of carbon material with a single atomic film thickness. The excellent permeability resistance and high thermal stability of graphene make graphene coatings have excellent anti-corrosion properties, and have great application potential as metal protective coatings. Kong [28] explored the corrosion resistance of Bis[3-(triethoxysilyl)propyl]tetrasulfide and graphene composite film on aluminum alloy by means of self-assembly and doping. The results shown that the composite film had a good protective effect on the aluminum alloy. GO is an intermediate product of the preparation of graphene by graphite oxidation. Compared with graphene, it is also a two-dimensional material with similar properties to graphene. The presence of oxygen-containing functional groups endows go with good dispersion and compatibility with polymers, etc. The outstanding aspect ratio of GO and its strong resistance to corrosive media can improve its corrosion resistance to matrix materials. Zhu [29] studied the corrosion resistance of 2024 aluminum alloy modified by organic material BTESPT/GO. It was found that the prepared composite film had good barrier ability to corrosive ions. However, it has been found that the corrosion resistance of the composite film of GO and polymer has only slightly increased, and there are few studies on the corrosion resistance and corrosion resistance mechanism of the composite film of micro-arc oxide film and GO and polymer.

In this paper, the microarc oxidation/Bis[3-(triethoxysilyl) propyl] tetrasulfide (BTESPT) /graphene oxide (MAO/BTESPT/GO) composite film was prepared by combining microarc oxidation and self-assembly on 6061 aluminum alloy. The morphology and composition of the composite film were tested by SEM and EDS. The salt spray test, Tafel polarization curve and electrochemical AC

impedance were used to test the corrosion resistance of the composite film. The results shown that the micro-arc oxidation/self-assembled composite film had excellent corrosion resistance.

2. MATERIAL AND METHODS

2.1 Preparation of sample and self-assembly liquid

A 6061 aluminum alloy substrate (the composition of which is shown in the following Table 1) was cut into a sample having a size of 30 mm × 40 mm × 2 mm, and mechanically ground with SiC sandpaper, and the sizes were 180 #, 600 #, 1000 #, and 1500 #, respectively. And it was removed the grease for one minute at 80℃, then ultrasonicated in distilled water and ethanol for 10 min. Next, use JHMAO-380/20A micro-arc oxidation power supply for micro-arc oxidation process, using pulse voltage method, the pulse frequency and duty cycle were set to 300Hz and 30% respectively. The pre-treated aluminum alloy substrate was used as an anode, and the stainless steel was used as a cathode in the electrolyte solution of the silicate solution, and a mixed electrolyte (9 g/L Na_2SiO_3, 4 g/L NaOH, 2 g/L $C_{10}H_{14}N_2O_8Na_2 \cdot 2H_2O$) was used. The sample was micro-arc oxidized for 30 min and the termination voltage was 300V. Finally, the sample treated by the micro-arc oxidation process was rinsed with distilled water and placed in a forced air oven at 50 °C for drying.

According to the volume ratio of BTESPT: distilled water: ethanol = 5: 5: 90, configure the total self-assembly liquid 100 mL, wherein acetic acid was used to adjust the pH of the mixed solution to 4, and the mixed solution was taken at 35℃. The magnetic stirrer was stirred for 2 h, then ultrasonically shaken at room temperature for 3 h, and the resulting solution was hydrolysed at room temperature for 48 hours. The graphene oxide suspension prepared by the Hummers method and the prepared BTESPT solution were ultrasonically mixed for 60 min in a ratio of 1:1, and the sample treated by the micro-arc oxidation process was self-assembled at a normal temperature for 1 h in the prepared self-assembly solution, and cured at 180℃ for 1 h. The preparation process was as shown in Fig. 1.

Table 1. The major compositions of AA 6061

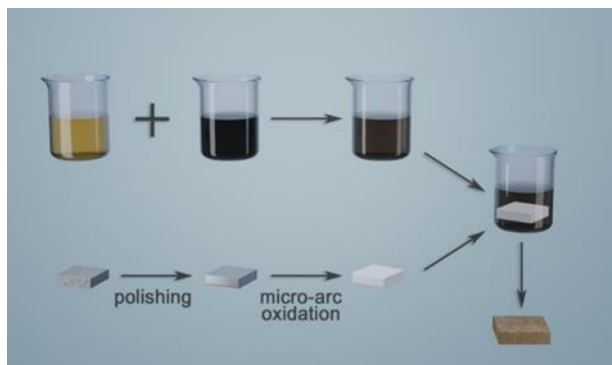| Elements	Cu	Mn	Mg	Zn	Cr	Ti	Si	Fe	Al
Contents(wt.%)	0.15-0.4	0.15	0.8-1.2	0.25	0.04-0.35	0.15	0.4-0.8	0.7	balance

Figure 1. Sample preparation flow chart

2.2 Test method

The surface morphology of the MAO/BTESPT/GO composite film was observed by Hitachi SU5000 scanning electron microscope (SEM) and energy color scatter line spectroscopy (EDS). Raman spectra was collected using a LabRam HR Raman system and the excitation source was a 780 nm laser with an extended scan between 100 and 3200 wavenumbers (10 seconds). The surface composition of the samples was analyzed with the ESCALAB 250xiXPS test system (with AlK sigma laser source at 1486.6eV). The electrochemical impedance of the sample was tested at room temperature using a three-electrode system (a saturated calomel electrode as a reference electrode, a platinum electrode as an auxiliary electrode, and an aluminum alloy sample as a working electrode) using a CHI860D electrochemical workstation. The test sample had an effective surface area of 1 cm^2 and the electrolyte was a 3.5% NaCl solution. The test was to soak the sample in a NaCl solution for half an hour to stabilize the open circuit potential (OCP) of the scanned sample, using a sinusoidal applied voltage of 10 mV and a frequency range of 10 mHz to 100 kHz. The scan rate of the test polarization curve was set to 1 mV•s^{-1}. After the test was completed, a series of data such as the corrosion current density of the sample were obtained and analyzed. Each test was performed 3 times under the same experimental conditions to ensure reproducibility of the test results. The corrosion resistance of the samples was tested using a salt spray tester model AC-60. In the salt spray box, the NaCl solution was 5% by mass, and the salt spray experiment was carried out in a 24-hour cycle using a continuous spray for 12 hours and a standing operation for 12 hours. The corrosion morphology of the sample was observed and photographed to observe the corrosion resistance of the sample.

3. RESULTS AND DISCUSSION

3.1 SEM analysis

The SEM of several different samples was shown in Fig. 2. The MAO film was shown in Fig. 2A. It can be observed that there were micropores and microcracks on the MAO film. The MAO/BTESPT/GO composite film was shown in Fig. 2B. The MAO/BTESPT composite film had a

compact structure, the micro-pores and micro-cracks on the micro-arc oxidation film were well sealed, forming a relatively uniform self-assembly film. However, the self-assembled film was usually very thin, and it was difficult to completely cover the micropores and microcracks on the micro-arc oxide film. Therefore, the tetrasulfide solution and the graphene oxide suspension were mixed in a ratio of 1:1 to prepare a self-assembled liquid to prepare a MAO/BTESPT/GO composite film on the surface of the aluminum alloy, which can well coat the MAO film. Microstructure diagram of aluminum alloy MAO/BTESPT/GO composite film was shown in Fig. 2C. It can be observed that the micropores and microcracks were completely covered and can well compensate for the defects in the MAO/BTESPT film. Wang [30] also discovered that micro-arc oxidation film also have micropore and micro-crack defects in the exploration of magnesium alloys. The BTESPT film was used to improve the defects of the micro-arc oxidation film, but the silane film also had relatively thin defects.
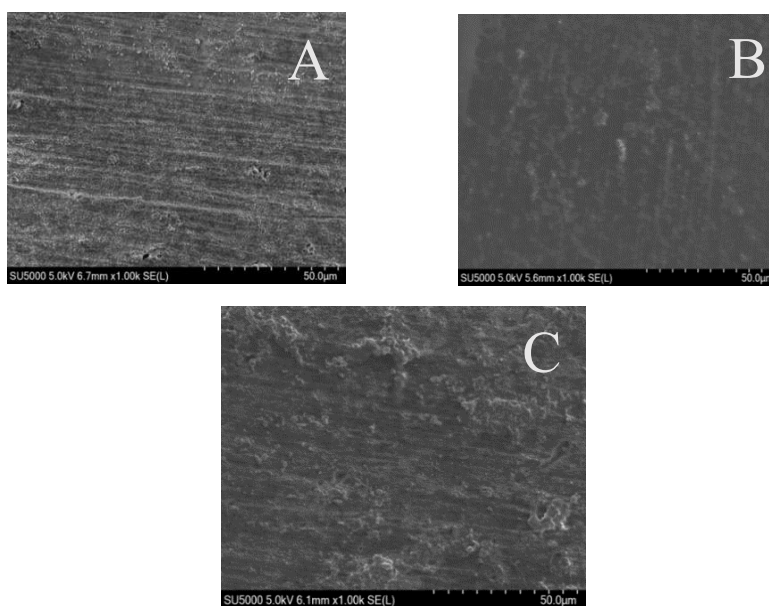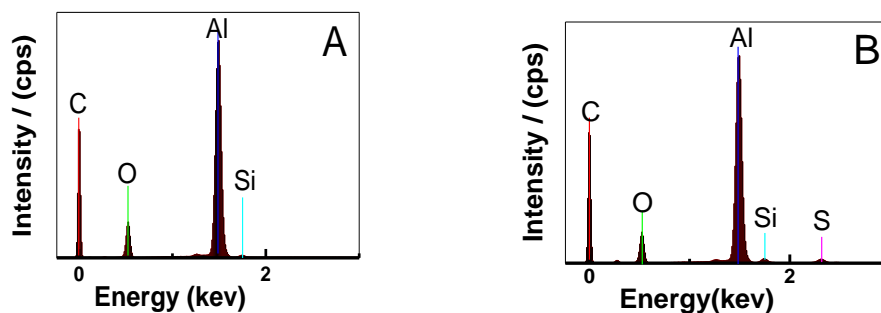

Figure 2. The results SEM of MAO film (A), MAO/BTESPT composite film (B) and MAO/BTESPT/GO composite film (C)
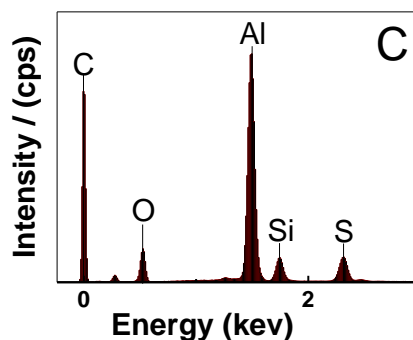
3.2 EDS analysis

Figure 3. The results EDS of MAO film (A), MAO/BTESPT composite film (B) and MAO/BTESPT/GO composite film (C)

Table 2. EDS data for the surface composition of samples

Sample	Al (weight%)	C (weight%)	O (weight%)	Si (weight%)	S (weight%)
MAO	55.71	4.29	39.14	0.86	----
MAO/BTESPT	48.35	14.88	34.13	1.50	1.15
MAO/BTESPT/GO	34.97	25.55	28.67	5.44	5.36

It can be concluded from Table 2 that the MAO/BTESPT/GO film was successfully prepared. It can be seen from the table that the contents of Al and O decreased sequentially, while the contents of C, Si and S increased sequentially, wherein S was a characteristic element of tetrasulfide. The MAO/BTEPT/GO composite film had a significantly higher content than the MAO/BTESPT film S, indicating that MAO/BTESPT/GO was well combined[28, 31]. Kong [28]reached a similar conclusion by measuring the EDS of BTESPT.

3.3 Raman analysis

In order to further verify the successful preparation of the MAO/BTESPT/GO composite film, the sample was further tested by Raman. As shown in Fig.4, characteristic peaks of graphene oxide can be observed, which were the D peak at about 1321 cm^{-1} and the G peak at 1590 cm^{-1}, respectively. The D peak was considered as the disordered vibration in the defective graphene and graphite (sp^3 defect), and the G peak of graphene was the main peak of graphene, which appeared due to the E$_{2g}$ mode of the sp^2 carbon domain, and represented the planar vibration of carbon atoms in crystalline graphite materials[32]. This indicated the successful preparation of go on micro-arc oxide film. A was formed by curing the MAO/BTESPT/GO composite film at 50℃, and B was formed by curing at 180 °C. It can be seen from the figure that the peak strength of the composite film at 180 °C was significantly stronger than 50℃, indicating that the composite film formed by curing at 180 °C was more preferable.
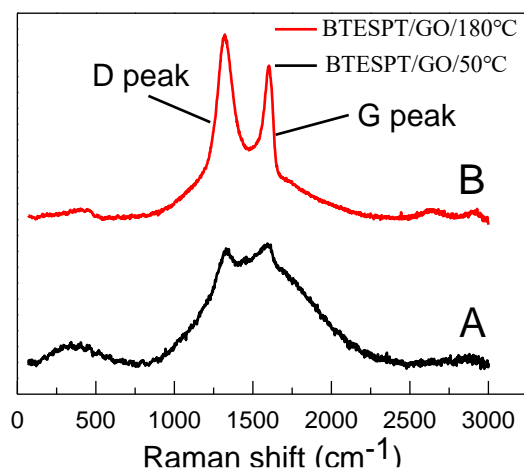
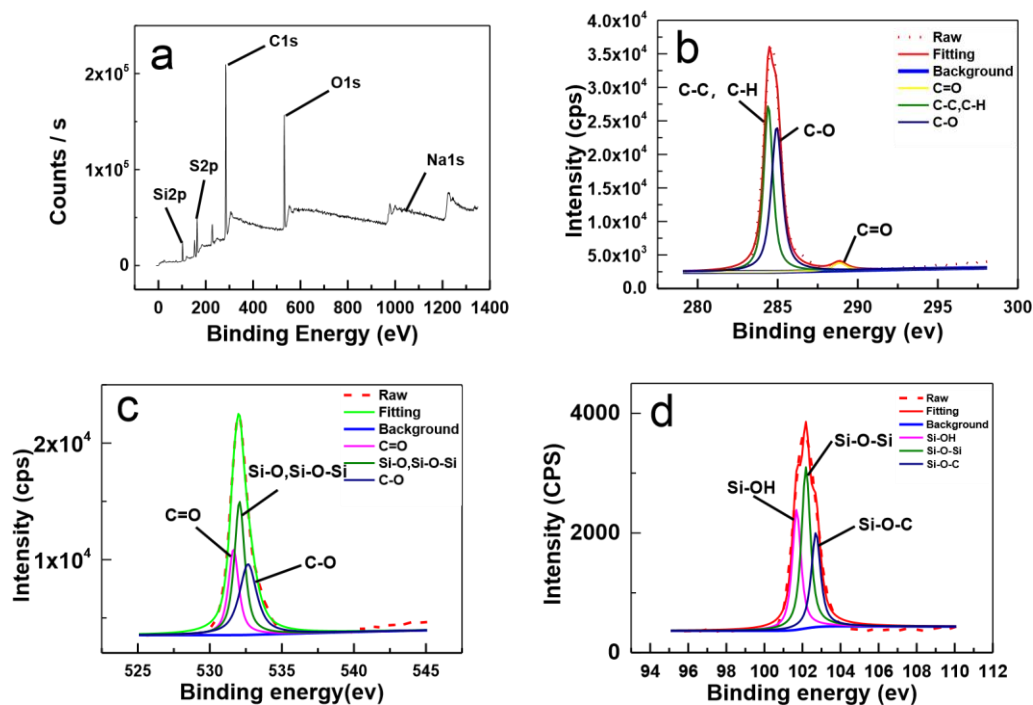**Figure 4.** The Raman of MAO/BTESPT/GO composite film

3.4 XPS

Figure 5. XPS results of wide-scan spectrum(a), C1s(b), O1s(c), Si2p(d) of MAO/BTESPT/GO composite film

The surface chemical composition of the aluminum alloy MAO/BTESPT/GO composite film was characterized by XPS. The full spectrum of XPS was shown in Fig.5a. From this figure, it can be seen that the surface of the composite film had Si, S, C, O, Na and other elements, indicating the successful preparation of the composite film, where S was the characteristic element of the tetrasulfide.

　　　　The Na element was derived from NaSiO₃, and the Si element may be derived from tetrasulfide or may be derived from NaSiO₃. The C1s spectrum was shown in Fig.5b. The original spectrum was fitted to three characteristic peaks centered at 284.60eV, 285.60eV and 288.87eV, which were C-C, C-O and C=O[29], respectively. This was similar to the conclusion that Zhu [29] found in XPS exploring the BTESPT/GO film. The existence of GO and BTESPT as self-assembly liquid on the micro-arc oxidation film of aluminum alloy was confirmed. The O1s spectrum was shown in. Fig.5c. The original spectrum was fitted to three characteristic peaks centered at 531.56eV, 531.94eV and 532.19eV, which were respectively C=O, Si-O (including Si-O-Si and Si-OH) and C-O, indicating that the reaction between graphene oxide and tetrasulfide was combined. Si the original spectrum was shown in Fig.5d. The original spectrum was fitted to three characteristic peaks centered at 101.32 eV, 102.08 eV and 102.83 eV, which corresponded to Si-OH, Si-O-Si and Si-O-C, respectively[29, 33]. Among them, Si-O-Si was formed by dehydration condensation reaction between tetrasulfides. Si-O-C was formed by dehydration condensation between a tetrasulfide molecule and an oxygen-containing functional group in graphene oxide. Their formation indicated that the composite film formed between tetrasulfide and graphene oxide covered the micro-arc oxidation film on the aluminum alloy.

3.5 Electrochemical performance

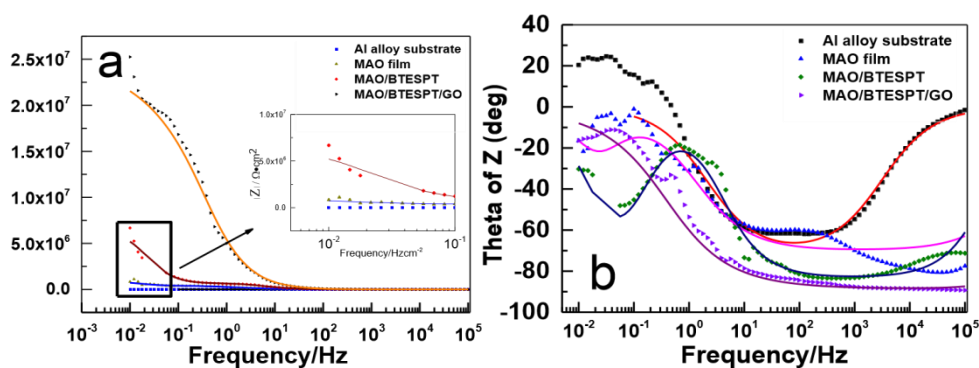### 3.5.1 Electrochemical impedance spectroscopy

Figure 6. the Bode chart of AC impedance: bode mold chart (a) bode phase angle chart (b) in a 3.5wt.
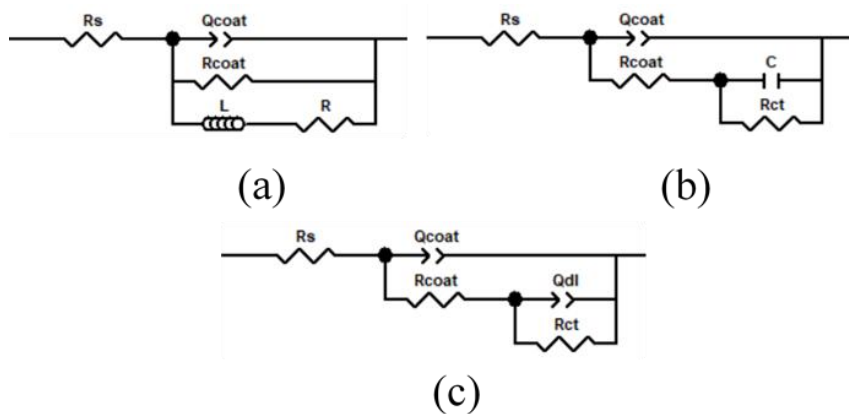% NaCl solution at room temperature

Figure 7. Equivalent circuit diagram of different samples: Aluminum alloy substrate(a), MAO film (b), MAO/BTESPT composite film and MAO/BTESPT/GO composite film (c)

Table 3. Fitting parameters of equivalent circuit diagrams of different samples

Sample	Rs ($\Omega \cdot cm^2$)	Qcoat (F/cm^2)	n_1	Rcoat ($\Omega \cdot cm^2$)	Qdl (F/cm^2)	n_2	Rct ($\Omega \cdot cm^2$)	C ($\Omega^{-1} cm^2$)
Al alloy substrate	10.7	3.501×0^{-5}	0.800	3662	--	--	--	--
MAO	9.00	4.80×10^{-7}	0.775	426110	--	--	4.11×10^5	2.47×10^{-5}
MAO/BTESPT	24.8	7.60×10^{-8}	0.924	710980	1.73×10^{-6}	0.991	5.52×10^6	--
MAO/BTESPT/GO	2.00	1.92×10^{-8}	0.984	118320	2.83×10^{-8}	0.460	2.48×10^7	--

The electrochemical impedance spectroscopy of the composite film was shown in Fig.6. The electrochemical impedance spectroscopy of different films of aluminum alloy matrix, MAO, MAO/BTESPT and MAO/BTESPT/GO was tested in 3.5% NaCl solution and the corrosion resistance of different film was investigated. It can be seen from Fig.6a. that the impedance variation range of different films in the high frequency range was not large. In the low frequency range, the MAO/BTESPT/GO composite film had a larger improvement than other film. The MAO/BTESPT/GO composite film (2.16×10^7 $\Omega \cdot cm^2$) in the low frequency (0.01Hz) range was an order of magnitude higher than MAO/BTESPT (5.19×10^6 $\Omega \cdot cm^2$), compared to MAO (8.26×10^5 $\Omega \cdot cm^2$) and aluminum alloy substrate (1.43×10^5 $\Omega \cdot cm^2$) increased by two orders of magnitude. It shown that the MAO/BTESPT/GO composite film acted as a corrosion-resistant aluminum alloy and hindered the corrosive medium. The results shown that the prepared MAO/BTESPT/GO composite film had better corrosion resistance than other films. The bode plot of phase angle in Fig.6b. also shown the differences among the aluminum alloy matrix, MAO, MAO/BTESPT and MAO/BTESPT/GO. The phase angle of MAO/BTESPT/GO in the high frequency range was generally higher than that of the aluminum alloy matrix, MAO, MAO/BTESPT and MAO/BTESPT/GO, indicating that the MAO/BTESPT/GO composite film had better protection effect.

The equivalent circuit diagram of the aluminum alloy substrate can be represented by Fig.7 (a), where R_s represented the liquid-to-liquid resistance between the research electrode and the reference electrode, which was affected by the electrolyte solution and the electrolytic cell. Q_{coat} represented the film capacitance, R_{coat} was the film resistance, and L was the inductive reactance. The equivalent circuit diagram of the aluminum alloy MAO film can be represented by Fig. 7(b), where C was an electric double film capacitor and R_{ct} was a charge transfer resistor. The equivalent circuit diagram of MAO/BTESPT and MAO/BTESPT/GO can be represented by Fig. 7(c), where Q_{dl} represented the capacitance of the electric double film [30].

According to the proposed equivalent circuit, the AC impedance spectrum was fitted, and the fitted data can be well matched with the experimentally measured AC impedance spectrum. The data obtained by fitting was listed in Table 3. R_{ct} was an important parameter to evaluate the properties of corrosive media. The larger the value, the better the electrochemical stability and corrosion resistance of the material. The R_{ct} value of the MAO/BTESPT/GO composite film was 2.4842×10^7 $\Omega \cdot cm^2$, which was two orders of magnitude higher than MAO (R_{ct} value was 4.1054×10^5 $\Omega \cdot cm^2$) compared to the MAO/BTESPT composite film (R_{ct} value was 5.5153×10^6 $\Omega \cdot cm^2$) was increased by an order of magnitude, indicating that the composite film can extremely improve the corrosion resistance of the aluminum alloy.
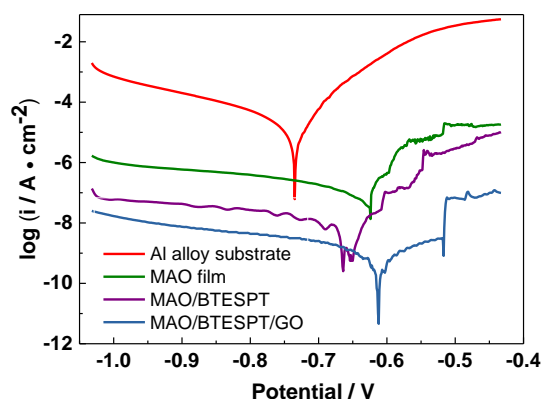
3.5.2 Polarization curve

Figure 8. Polarization curves of four samples in 3.5wt.% NaCl solution

The linear polarization curves of the aluminum alloy matrix, MAO, MAO/BTESPT and MAO/BTESPT/GO self-assembled composite films were shown in Fig. 8. The data obtained from the linear polarization curve analysis were shown in Table 4. It can be seen from Table 4 that the corrosion current density of the MAO/BTESPT/GO composite film was less than the corrosion current density of the MAO film. The corrosion current density of the MAO/BTESPT/GO composite film was reduced by five orders of magnitude compared to the corrosion current density of the aluminum alloy substrate, and the corrosion current density of the MAO and MAO/BTESPT film was reduced by four and one order of magnitude, respectively. The corrosion potential represented the degree of corrosion that occurred,

and the more positive the corrosion potential, the less likely the corrosion behavior occurred. Compared with the simple aluminum alloy matrix and the MAO film, the MAO/BTESPT/GO composite film had a more corrosive potential, thereby improving its corrosion resistance [34-37].

Table 4. Analysis of Polarization Curve Data of Four Samples in 3.5wt.% NaCl Solution

Sample	E_{corr} (V)	I_{corr} (A·cm^{-2})
Matrix	-0.74	1.42×10^{-5}
MAO	-0.63	4.72×10^{-6}
MAO/BTESPT	-0.66	7.79×10^{-9}
MAO/BTESPT/GO	-0.61	8.27×10^{-10}

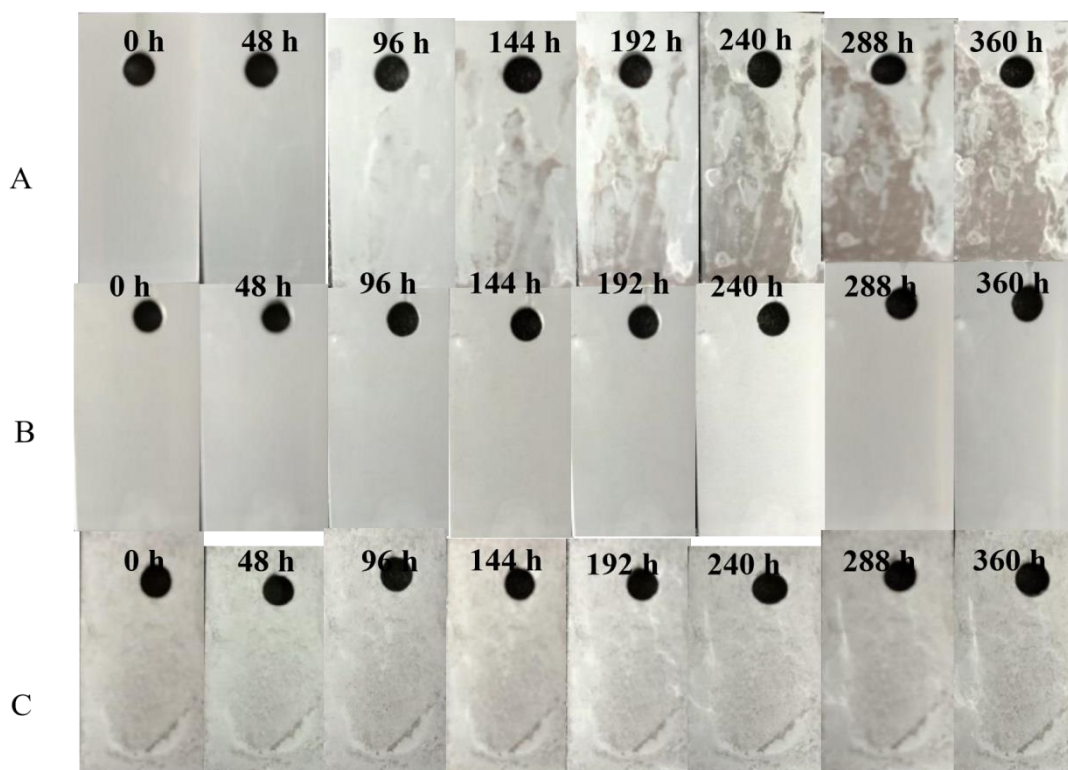*3.5.3 Neutral salt spray experiment*

Figure 9. Salt spray corrosion pictures of different samples at different times: MAO film (A) MAO/BTESPT composite film (B) MAO/BTESPT/GO composite film (C)

The salt spray experimental pictures of aluminum alloy MAO (A), MAO/BTESPT (B) composite film and MAO/BTESPT/GO (C) composite film at different times were shown in Fig. 9. It can be seen from Fig. 9(A) that pitting corrosion appeared on the surface of MAO film after 96 hours of salt spray,

and with the extension of salt spray test time, the area of the sample of single micro-arc oxide film expanded, micro-arc oxidation the film sample was destroyed and the corrosion was very severe. It can be seen from Fig. 9(B) that the MAO/BTESPT composite film had a certain corrosion phenomenon after 96h, but with the extension of the salt spray time, the corrosion of the film developed slowly and there was almost no corrosion phenomenon. It can be seen from Fig. 9 (C) that the MAO/BTESPT/GO composite film also presented pitting corrosion after 96h. Like the MAO/BTESPT composite film, the corrosion of the film developed slowly with the extension of the salt spray time, and there was almost no corrosion. It shown that the MAO/BTESPT and MAO/BTESPT/GO composite films can resist corrosion compared to a single micro-arc oxide film. Based on the electrochemical tests of different films of Fig.6. and Fig.8. It can be concluded that the MAO/BTESPT/GO composite film had better corrosion resistance than the MAO/BTESPT film and the MAO film, and its corrosion resistance was better.

4. CONCLUSIONS

In this paper, microarc oxidation, graphene oxide and (Bis [3-(triethoxysilyl) propyl] tetrasulfide BTESPT)(MAO/BTESPT/GO) composite films were prepared by combining microarc oxidation with self-assembly. The morphology and composition of the composite film was tested by SEM and EDS. The salt spray test, Tafel polarization curve and electrochemical AC impedance were used to test the corrosion resistance of the composite film. The results shown that the MAO/BTESPT/GO composite film was dense and had the function of sealing micropores and microcracks in the micro-arc oxidation film. The impedance of the composite film was much larger than that of the aluminum alloy matrix and other films. The composite film had good corrosion resistance and achieved the purpose of improving the corrosion resistance of the aluminum alloy.

CONFLICT OF INTEREST
The authors declare no conflict of interest.

References

1. Y. Chi, G. Gu, H. Yu, C. Chen, *Optics & Lasers in Engineering.,* 100 (2018) 23.
2. J.-l. Hu, Y.-p. Yi, S.-q. Huang, *J. Cent. South Univ.,* 21(2014) 2612.
3. T. Monetta, A. Acquesta,V. Maresca, R. Signore, F. Bellucci, P. Di Petta, M. Lo Masti, *Handb. Surf. Interface Anal.,* 45 (2013) 1522.
4. Y. Liao, Y. Li, Q. Pan, M. Huang, C. Zhou, *Eng. Fract. Mech.,* 194 (2018) 262.
5. B. Priet, G. Odemer, C. Blanc, K. Giffard, L. Arurault, *Surf. Coat. Technol.*, 307 (2016) 206.
6. L. Khazanov, Aluminum: Alloys, *Metall.,* 59 (2016) 856.
7. N.A. Jingxin, M.U. Wenlong, G. Qin, W. Tan, L. Pu, *Int. J. Adhes. Adhes.*, 85 (2018) 138.
8. A.Bałkowiec,J. Michalski, H. Matysiak, K.J. Kurzydlowski, *Mater. Sci.-Pol.,* 29 (2011) 305.

9. I. Schoukens, F. Cavezza, J. Cerezo, V. Vandenberghe, V.C. Gudla, R. Ambat, *Mater. Corros.*, 69 (2018) 881.
10. L.B. Boinovich, K.A. Emelyanenko, A.G. Domantovsky, A.M. Emelyanenko, *Langmuir.,*34(2018) 7059.
11. M. Vakili-Azghandi, A. Fattah-alhosseini, M.K. Keshavarz, *Meas.,* 124 (2018) 252.
12. A. Esmaeilirad, M.V. Rukosuyev, M.B.G. Jun, F.C.J.M.V. Veggel, *Surf. Coat. Technol.,* 285 (2016) 227.
13. Y.Q. Wen, H.M. Meng, S.*, Surf. Coat. Technol.,* 258 (2014) 574.
14. V. Dalmoro, J.H.Z.D. Santos, E. Armelin, C. Alemán, D.S. Azambuja, *Corros. Sci.,* 60 (2012) 173.
15. M. Vippola, S. Ahmaniemi, J. Keränen, P. Vuoristo, T. Lepistö, T. Mäntylä, E. Olsson, *Mater. Sci. Eng A.,* 323 (2002) 1.
16. Z. Zeng, A. Liang, J. Zhang, *Electrochim. Acta,* 53 (2008) 7344.
17. J.V. Kloet, W. Schmidt, A.W. Hassel, M. Stratmann, *Electrochim. Acta,* 48 (2003) 1211.
18. K.W. Cho, V.S. Rao, H.S. Kwon, *Electrochim. Acta,* 52 (2007) 4449.
19. J. Zhao, L. Xia, A. Sehgal, D. Lu, R.L. Mccreery, G.S. Frankel, *Surf. Coat. Technol.,* 140 (2001) 51.
20. M. Narozny, K. Zakowski, K. Darowicki, *Corros. Sci.,* 98 (2015) 605.
21. R. Najjar, S.A. Katourani, M.G. Hosseini, *Prog. Org. Coat.,* 124 (2018) 110.
22. A. Renaud, M. Poorteman, J. Escobar, L. Dumas, Y. Paint, L. Bonnaud, P. Dubois, M.-G. Olivier, *Prog. Org. Coat.,* 112 (2017) 278.
23. L. Shi, Y. Xu, K. Li, Z. Yao, S. Wu, *Current Applied Physics.*, 10 (2010) 719.
24. Z.-Y. Ding, L.-Y. Cui, X.-B. Chen, R.-C. Zeng, S.-K. Guan, S.-Q. Li, F. Zhang, Y.-H. Zou, Q.-Y. Liu, *J. Alloys Compd.,* 764 (2018) 250.
25. L.-j. Bai, G. Kou, K. Zhao, G.-t. Chen, F.-x. Yan, *J. Alloys Compd.,* 775 (2019) 1077.
26. X. Zhan, W. Shang, Y. Wen, Y. Li, M. Ma, *J. Alloys Compd.,* 774 (2019) 522.
27. R. Arrabal, M. Mohedano, E. Matykina, A. Pardo, B. Mingo, M.C. Merino, *Surf. Coat. Technol.,* 269 (2015) 64.
28. Y. Wen, D. Kong, W. Shang, M. Ma, X. Zhan, Y. Li, *Colloids Surf., A.,* 562 (2019) 247.
29. H. Zhu, L. Yue, C. Zhuang, Y. Zhang, X. Liu, Y. Yin, S. Chen, *Surf. Coat. Technol.,* 304 (2016) 76.
30. W. Shang, *Int. J. Electrochem. Sci.,* 12 (2017) 11875.
31. Y. Dun, Y. Zuo, *Appl. Surf. Sci.,* 416 (2017) 492.
32. Y.-q. Wen, H.-m. Meng, W. Shang, *RSC Adv.,* 5 (2015) 80129.
33. Y. Q. Wen, *Int. J. Electrochem. Sci.,* 14 (2019) 6018.
34. J. Liu, L. Hua, S. Li, M. Yu, *Appl. Surf. Sci.,* 327 (2015) 241.
35. S. Ding, T. Xiang, C. Li, S. Zheng, J. Wang, M. Zhang, C. Dong, W. Chan, *Mater. Des.,* 117 (2017) 280.
36. Y. Liu, J. Zhang, S. Li, Y. Wang, Z. Han, L. Ren, *RSC Adv.,* 4 (2014) 45389.
37. S. Mokhtari, F. Karimzadeh, M.H. Abbasi, K. Raeissi, *Surf. Coat. Technol.,* 324 (2017) 99.